One-Equation Turbulence Model of Spalart and Allmaras in Supersonic Separated Flows

Henry Y. Wong*
European Space Agency,
2200 AG Noordwijk, The Netherlands

Introduction

SUPERSONIC separated flows take place in many engineering applications, and in many cases, the state of the separated flow is unknown. It could be laminar, transitional, or fully turbulent. The one-equation turbulence model of Spalart and Allmaras[1] (SA) has a feature to allow the existence of a stable laminar solution. In other words, the eddy viscosity $\nu_t = 0$ is a stable solution. This implies that if the flowfield is laminar the SA model can predict a laminar solution. The SA model has a trip term to initiate transition in a smooth manner. This kind of transition is mainly numerical and has little to cope with the boundary layer's natural tendency to transition based on local pressure gradients, suction, wall roughness, and so on. The application of the trip term is almost exclusively for a situation where the flow upstream of the trip point is laminar. Downstream, far away from the trip point, this term has no influence on the solution. It is important to realize that, in the case of relaminarization, the transition process from turbulence to laminar depends mainly on the balance of the production, diffusion, and destruction terms and is independent of the trip point location upstream provided it is far from the location where relaminarization takes place. Having said this, because the model does not include any physical argument on the onset of transition, the model is at best able to predict relaminarization but cannot be trusted to predict accurately the onset and duration of transition. Nevertheless, this is still better than employing an algebraic model, such as that of Baldwin and Lomax[2] (BL), which cannot predict relaminarization except in the case where a correct number for the BL parameter C_{MUTM} is known a priori. This parameter is to suppress the incorrectly large eddy viscosity generated by strong local velocity gradients and is a function of local Reynolds number. It is important to make sure that this parameter does not suppress the correct large eddy viscosity. Two examples are given in this Note to demonstrate the preceding discussion. Each example is calculated first with the BL model, which is then used as an initial solution with the SA model. The objective of this procedure is to see whether in a laminar flowfield a fully turbulent flow created by the BL model can be relaminarized by the SA model.

An initial solution for the SA model can be obtained from a solution with the BL model by converting the eddy viscosity from the BL solution, ν_t, to the transformed eddy viscosity $\bar{\nu}$ in the SA model, where inside the boundary layer

$$\nu_t = \bar{\nu} f_{v1}, \qquad f_{v1} = \frac{\chi^3}{\chi^3 + c_{v1}^3}, \qquad \chi = \frac{\bar{\nu}}{\nu} \tag{1}$$

and outside the boundary layer

$$\nu_t = \bar{\nu} \tag{2}$$

In practice, one can specify a value for the kinematic viscosity ν to switch from Eq. (1) to Eq. (2). Equation (1) can be solved for $\bar{\nu}$, which gives

$$\bar{\nu} = \frac{\nu_t}{4} + \frac{a}{2} + \frac{\sqrt{\left(\nu_t^2/2\right) + a\nu_t - b + 2\sqrt{4c_{v1}^3\nu^3\nu_t + b^2}}}{2} \tag{3}$$

where

$$a = \sqrt{\frac{\nu_t^2}{4} + b}, \qquad b = \frac{c - e\nu_t^2}{4e}$$

$$c = e\nu_t^2 - 73728^{\frac{1}{3}} c_{v1}^3 \nu^3 \nu_t + \left(\frac{32}{243}\right)^{\frac{1}{3}} e^2$$

$$e = \left[\sqrt{2304 c_{v1}^6 \nu^6 f + f^2} - f\right]^{\frac{1}{3}}, \qquad f = 243 c_{v1}^3 \nu^3 \nu_t^3$$

From past experience with attached flow simulations, this methodology usually gives a converged solution faster than the way suggested by the authors of the model in Ref. 1. However, in the case of separated flows, this methodology does not gain much in convergence because of the large differences between the solutions from the BL and the SA models. Nevertheless, this is still a much more robust way than starting with $\bar{\nu} = 0$ uniformly in the initial solution, which is quite unstable in some cases. Furthermore, in the case of high Reynolds numbers, it is sufficient to apply Eq. (2) everywhere because χ is large except in a very thin layer at the wall.

Results

The SA model was incorporated into the finite volume Navier–Stokes code of Wong,[3] which has been used extensively in many turbulence simulations with attached and separated flows. Only the grid-converged solutions are presented here. Each example has a total number of grid points of around 40,000. The first example is an axisymmetric contour nozzle with a reservoir pressure of 26.8 bar and a total temperature of 310 K. At the exit of the nozzle, the boundary condition is subjected to an external static pressure of 75 KPa. In the turbulence simulations, the location of turbulence onset is set at just after the throat of the nozzle.

Figure 1 presents the streamlines of three different calculations: laminar, turbulent with the BL model,[4] and turbulent with the SA model. The numbers shown at the exit end are Mach numbers. Figure 2 shows the experimental observation at the nozzle exit. The experiment was done by L. Custer in the National Aerospace Laboratory in The Netherlands. The flow has been carefully observed for longer than a minute, and no sign indicates that the flow is unsteady. By comparing the two figures, one can see that the experiment shows that the flow separates somewhere between the solutions from the laminar and the turbulent with the SA model. The flow separation begins at 3 ± 0.4, 17 ± 0.4, and 8 ± 0.4 mm from the nozzle exit for the laminar, the BL turbulent, and the SA turbulent cases, respectively. In fact, the experimental result with a separation started at 5 ± 1 mm from the nozzle exit (projected from Fig. 2) is closer to the laminar solution than to the SA turbulent solution. Even though the SA model starts off with a fully turbulent flow solution from the BL model, it still predicts a laminar solution after the throat, which evolves gradually downstream to become transitional or turbulent near the nozzle exit. This demonstrates that the SA model can cope with relaminarization, whereas the BL model assumes that the flowfield is fully turbulent after the throat, which renders a large flow

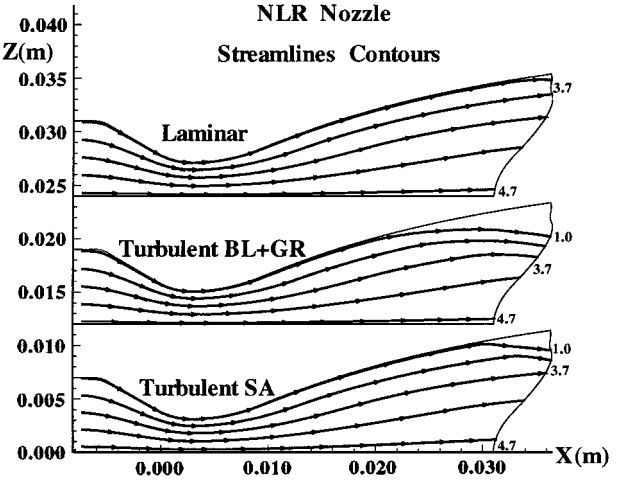

Fig. 1 Numerical streamlines inside a cold nozzle flow: GR, Granville theory.

Received March 11, 1998; revision received Oct. 22, 1998; accepted for publication Nov. 7, 1998.

*Atos Consultant, European Space Research and Technology Center, P.O. Box 299. Member AIAA.

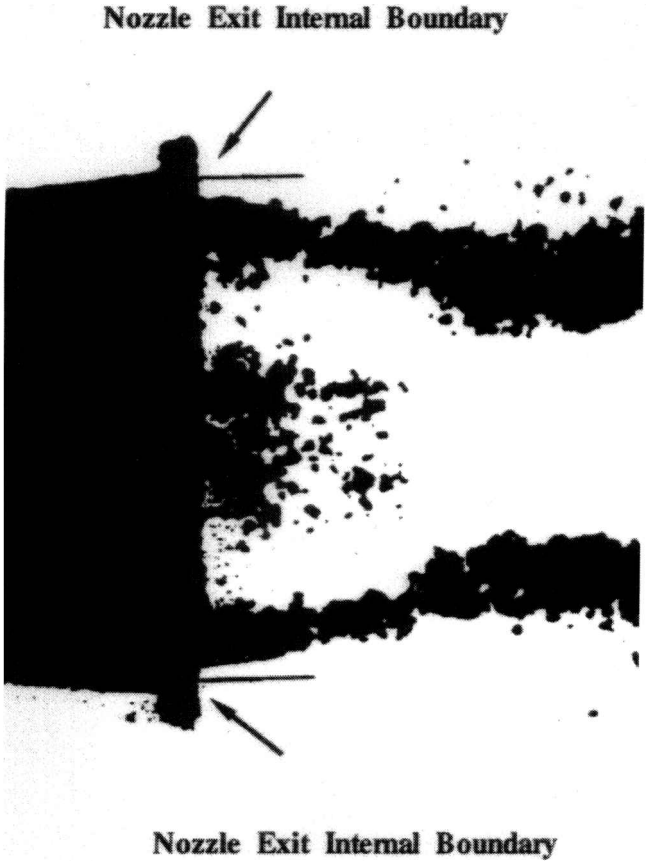

Fig. 2 Experimental observation at the nozzle exit.

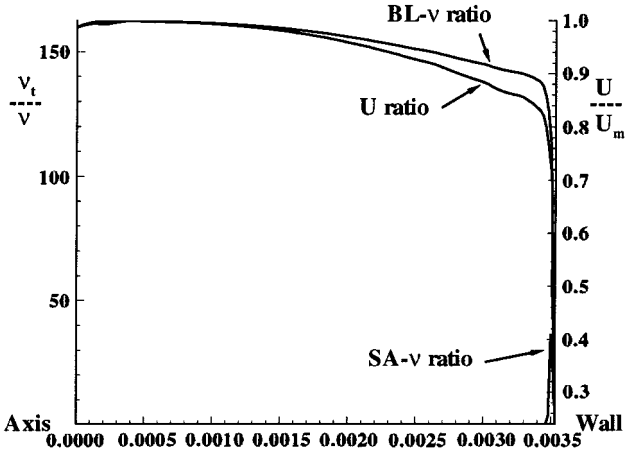

Fig. 3 Viscosity ratio comparison downstream from nozzle throat.

separation. Moreover, by tuning the parameter C_{MUTM} in the BL model to 70 instead of 14, the BL solution tends to behave like the SA solution. Figure 3 shows a comparison between the BL and SA solutions in terms of viscosity ratio (kinematic eddy/kinematic). The velocity profile gives a guidance to the local boundary-layer thickness. This is taken at a station farther downstream from the throat of the nozzle. Clearly, the SA solution diminishes the BL viscosity ratio to almost zero in most of the flow between the wall and the axis. However, in the inner part of the boundary layer, the SA model fails to diminish the eddy viscosity below the laminar viscosity. Nevertheless, the core flow still behaves more like laminar than turbulent flow. The degree of relaminarization in the SA model is significant enough to capture laminar flow behavior. The discrepancy between the SA solution and the experiment is mainly attributed to the lack of a physical transition model in the SA model. Moreover, the model does not include the compressibility effect and has not been validated at all with any axisymmetric configuration. In other words, the closure coefficients in the SA model are not universal, as mentioned in Ref. 1. This will be demonstrated further in the second example.

Table 1 Physical freestream conditions

Mach	Re/m	T_0, K	T_{wall}, K	L_{ref}, m
6.85	14.8×10^6	600	296	0.05924

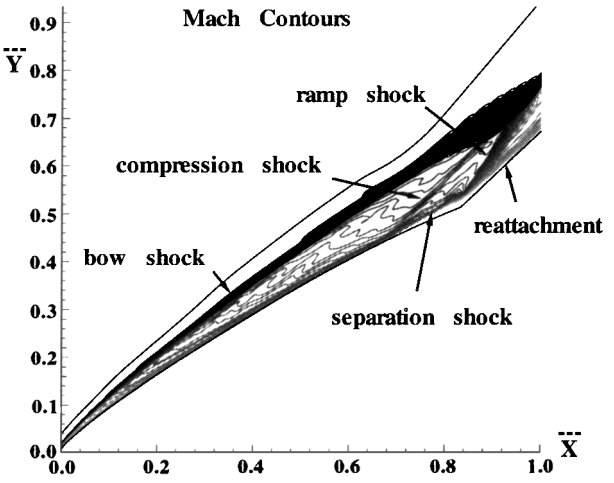

Fig. 4 Mach contours showing multiple shock locations in the flow structure.

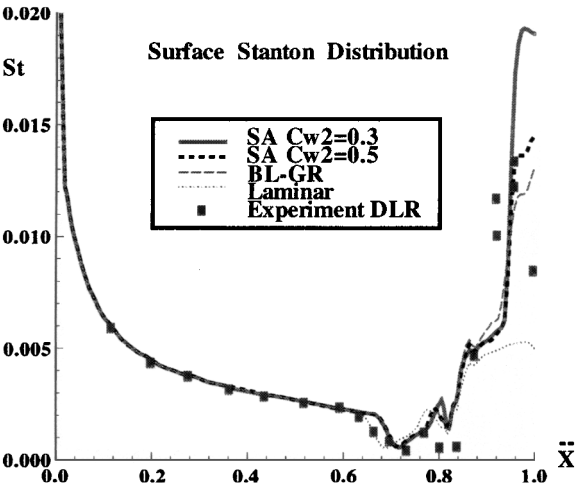

Fig. 5 Wall Stanton number along the surface of hyperboloidal-flare: GR, Granville theory.

The second example is an axisymmetric hyperboloidal flare, which has been presented in the First U.S.–Europe High Speed Flowfield Database Workshop, Part 2; more detail can be found in Ref. 3. The freestream conditions are indicated in Table 1.

Figure 4 shows the multiple shock locations in the flow structure. The objective is to examine the sensitivity of the closure coefficients in the SA model to the heating at the reattachment. We assume that the onset of transition is at the reattachment.

Figure 5 presents the distribution of Stanton numbers at the wall along the surface of the hyperboloidal flare. The experiment was done by Krogmann at the German Aerospace Laboratory (DLR), Göttingen, Germany, and more information can be found in Ref. 5. By comparing the numerical data with the experiment, one can see that the flow is either transitional or fully turbulent at the reattachment, which justifies the assumption of the location of transition onset. The difference between the solutions from the BL model and the SA model is not large because the selected location for the onset of transition or turbulence is about right. This test case is very sensitive to skin friction, which determines the onset of separation and the heating at reattachment. There are two SA solutions in Fig. 5, each corresponding to a different value in $Cw2$, which is a closure coefficient in the SA model that controls the skin friction and has been validated with a standard flat plate. The original value of $Cw2$ given by the authors of the model in Ref. 1 is 0.3, which overpredicts the heating by approximately 40% at the reattachment.

By tuning the coefficient to 0.5, it shows better agreement with the experimental data. Because of insufficient measurement data along the reattachment, there is still some uncertainty in the peak Stanton value in that region. Nevertheless, this certainly is not the means to solve the problem. The main difficulty in this problem is to establish a physical transition model at the reattachment. Moreover, applying an incorrect transition model at the reattachment renders an incorrect onset of separation upstream, as shown in Fig. 5 at $\bar{X} = 0.64$.

Conclusion

The prediction of relaminarization with the SA model has been demonstrated with an axisymmetric configuration that has not been validated by the authors of the model in Ref 1. The sensitivity of the closure coefficients is highlighted, and more research is required to validate the SA model before it can be used universally with any configuration. Because of the lack of a physical transition model in the SA model, care has to be taken in the uncertainty in the prediction of transition onset and duration with this model. In addition, the compressibility effect has not been taken into account in this model.

References

[1]Spalart, P. R., and Allmaras, S. R., "A One-Equation Turbulence Model for Aerodynamic Flows," AIAA Paper 92-0439, Jan. 1992.

[2]Baldwin, B. S., and Lomax, H., "Thin Layer Approximation and Algebraic Model for Separated Turbulent Flows," AIAA Paper 78-0257, Jan. 1978.

[3]Wong, H., "Hypersonic Flow over a Hyperboloidal-Flare," *Proceedings of the First Europe–US High Speed Flow Field Database Workshop Part 2*, Italian Aerospace Research Centre (to be published).

[4]Granville, P. S., "Baldwin–Lomax Factors for Turbulent Boundary Layers in Pressure Gradients," *AIAA Journal*, Vol. 25, No. 12, 1987, pp. 1624–1627.

[5]Krogmann, P., "Calibration and Validation Measurements in the Ludwieg Tube Tunnel B (RWG)," DLR Göttingen, Rept. ESA/CNES HT-TR-E-1-301-DGLR, Göttingen, Germany, Aug. 1995.

C. G. Speziale
Associate Editor

Wake Generation Compressibility Effects in Unsteady Aerodynamics

Ronald J. Epstein* and Donald B. Bliss†
Duke University, Durham, North Carolina 27708-0300

Introduction

THE phenomena of wake generation and evolution are the subject of continued research[1–8] and development. When dealing with either conventional fixed-wing aircraft or rotorcraft, the wake formation and subsequent dynamics are important issues. The behavior of the wake can profoundly affect aerodynamic loading, induced wash, and aerodynamic noise. In some situations the assumptions of an incompressible (constant-density) wake flow facilitates aerodynamic modeling. This assumption is particularly beneficial for three-dimensional, free-wake analysis, where motion and deformation of the wake under its own influence is to be determined.[6,7] Free-wake analysis is commonly used in rotorcraft aerodynamic models. Typically, the wake is discretized into vortex elements connected to form vortex filaments and/or vortex sheets. The velocity field from these elements is computed using the Biot–Savart law, which restricts the validity of the wake representation to incompressible constant-density flow. That the wake convects with the surrounding fluid and induces flow velocities that have very low Mach numbers appears to support the accuracy of the incompressible flow assumption. It is, therefore, not unusual to find rotorcraft aerodynamic analyses that embody compressibility effects in the blade aerodynamics model but utilize an incompressible free-wake analysis.

A criticism of this approach is that, although the wake-induced velocities may be low, the relative velocities between the wake and the generating blade, and subsequent blades the wake may encounter, may correspond to relatively high subsonic Mach numbers. During the unsteady wake generation process, waves generated both on the airfoil and in the wake itself travel both upstream and downstream, and the finite propagation speed (especially the slower upstream wave) may introduce significant phase delays in comparison with an incompressible case that has infinite wave speed. The implications of coupling an incompressible wake to a compressible blade aerodynamics analysis have not been systematically explored, even though this approach has been repeatedly undertaken in practice as an expedient to the formulation of a complex problem.

The present research illustrates the role of wake compressibility for the relatively simple case of a wake generated by a two-dimensional unsteady airfoil, as a first step toward exploring the effect of the wake incompressibility assumption. Even this relatively simple case will be seen to provide considerable physical insight. From this, a criterion for wake compressibility is derived. The derivation, from fundamental physical principles, also includes a discussion of the fundamental length and timescales that appear in the problem.

To illustrate the derived wake compressibility criterion, numerical results are presented for a model unsteady compressible aerodynamic calculation, namely a flat-plate airfoil encountering a harmonic nonuniform inflow. This is a compressible form of the von Kármán–Sears problem.[9,10] Through this simple example, it is demonstrated that wake compressibility can indeed have a profound effect on unsteady aerodynamic and aeroacoustic calculations.[11,12] It is also shown that only a small portion of the wake, that which is closest to the trailing edge of the lifting surface, is important with regard to wake compressibility. Therefore, the criterion derived can be regarded as a correction to existing wake analysis schemes as opposed to a replacement for them and, as demonstrated, can be effectively used as such.

Wake Compressibility Criterion

Consider a two-dimensional wing section (Fig. 1a), translating in the $-x$ direction with velocity V_∞ subject to an unsteady excitation. The excitation can be due to unsteady heave, pitch, or gust and is not limited to the frequency domain. An unsteady wake is, therefore, shed from the trailing edge of the wing section. The wake is composed of both positive and negative vorticity, as shown schematically in Fig. 1a. The sign and magnitude of the vorticity in the wake acts as an effective fluidic memory for the unsteady changes of vorticity, upwash, and pressure on the surface of the wing section and must satisfy Kelvin's theorem.

This Note investigates the aeroacoustic aspects of the wake as it is generated at the trailing edge. It is assumed that the wake is continuously shed both temporally and spatially. Therefore, in any small increment of time, a small increment of wake is shed and convects from the trailing edge. The detailed viscous mechanism of the shedding process[13] is not addressed. Rather, the global aeroacoustics of the wake inception is investigated.

Looking at Fig. 1a, consider a small increment of wake being shed. Simultaneously, a sound wave is emitted at the trailing edge from the unsteady disturbance induced by a newly shed wake increment. The sound wave is generated by the final adjustment of the flowfield at the trailing edge. In terms of potential flow or panel methods,[14–19] this is the last adjustment made in the surface potential strength distribution (source or doublet), at the trailing edge, before the local jump in potential is shed into the wake. The value of the jump in potential at the trailing edge is then convected downstream in the wake. This is equivalent to satisfying Kelvin's theorem.

Received July 12, 1996; revision received June 18, 1998; accepted for publication July 8, 1998.

*Research Assistant Professor, Department of Mechanical Engineering and Material Science, School of Engineering; currently Project Engineer, Phantom Works, The Boeing Company, Mailcode S1067126, P.O. Box 516, St. Louis, MO 63166-0516. Member AIAA.

†Associate Professor, Department of Mechanical Engineering and Material Science, School of Engineering. Member AIAA.